

Estimation of the deleterious genomic mutation rate

If we use  $1 - (K_d/K_s)$  as a measure of the fraction of mutations in protein-coding genes that are deleterious (for *Caenorhabditis*,  $K_d/K_s \approx 0.06$ )<sup>24</sup> and multiply this by the genomic rate of nonsynonymous base substitution mutations in exon sequences in the MA lines (0.18 nonsynonymous mutations per genome per generation, given that ~26% of the *C. elegans* genome is exon, ~75% of exon nucleotides are nonsynonymous sites, and our total mutation rate of 0.9 base substitutions per genome per generation), we get 0.17 as an estimate of  $U_d$  for *C. elegans*. Adding the rate of indel mutations in exon sequence (0.31 indel mutations in exons per genome per generation, given that ~26% of the *C. elegans* genome is exon and our total mutation rate of 1.2 indels per genome per generation) and assuming all exon indels are deleterious, yields 0.48 as an estimate of  $U_d$  for *C. elegans*.

Received 3 February; accepted 1 June 2004; doi:10.1038/nature02697.

1. Drake, J. W., Charlesworth, B., Charlesworth, D. & Crow, J. F. Rates of spontaneous mutation. *Genetics* **148**, 1667–1686 (1998).
2. Nachman, M. W. & Crowell, S. L. Estimate of the mutation rate per nucleotide in humans. *Genetics* **156**, 297–304 (2000).
3. Kumar, S. & Subramanian, S. Mutation rates in mammalian genomes. *Proc. Natl Acad. Sci. USA* **99**, 803–808 (2002).
4. Robertson, H. M. The large *srh* family of chemoreceptor genes in *Caenorhabditis* nematodes reveals processes of genome evolution involving large duplications and deletions and intron gains and losses. *Genome Res.* **10**, 192–203 (2000).
5. Witherspoon, D. J. & Robertson, H. M. Neutral evolution of ten types of mariner transposons in the genomes of *Caenorhabditis elegans* and *Caenorhabditis briggsae*. *J. Mol. Evol.* **56**, 751–769 (2003).
6. Vassilieva, L. L., Hook, A. M. & Lynch, M. The fitness effects of spontaneous mutations in *Caenorhabditis elegans*. *Evolution* **54**, 1234–1246 (2000).
7. Denver, D. R., Morris, K. & Thomas, W. K. Phylogenetics in *Caenorhabditis elegans*: an analysis of divergence and outcrossing. *Mol. Biol. Evol.* **20**, 393–400 (2003).
8. Denver, D. R., Morris, K., Lynch, M., Vassilieva, L. L. & Thomas, W. K. High direct estimate of the mutation rate in the mitochondrial genome of *Caenorhabditis elegans*. *Science* **289**, 2342–2344 (2000).
9. Ochman, H. Neutral mutations and neutral substitutions in bacterial genomes. *Mol. Biol. Evol.* **20**, 2091–2096 (2003).
10. Petrov, D. A., Lozovskaya, E. R. & Hartl, D. L. High intrinsic rate of DNA loss in *Drosophila*. *Nature* **384**, 346–349 (1996).
11. Petrov, D. A. & Hartl, D. L. Pseudogene evolution and natural selection for a compact genome. *J. Hered.* **91**, 221–227 (2000).
12. Hirotsune, S. *et al.* An expressed pseudogene regulates the messenger-RNA stability of its homologous coding gene. *Nature* **423**, 91–96 (2003).
13. Yamada, K. *et al.* Empirical analysis of transcriptional activity in the *Arabidopsis* genome. *Science* **302**, 842–846 (2003).
14. Balakirev, E. S. & Ayala, F. J. Pseudogenes: are they 'junk' or functional DNA? *Annu. Rev. Genet.* **37**, 123–151 (2003).
15. Charlesworth, B. The changing sizes of genes. *Nature* **384**, 315–316 (1996).
16. Lynch, M. & Conery, J. S. The origins of genome complexity. *Science* **302**, 1401–1404 (2003).
17. Marais, G., Mouchiroud, D. & Duret, L. Does recombination improve selection on codon usage? Lessons from nematode and fly complete genomes. *Proc. Natl Acad. Sci. USA* **98**, 5688–5692 (2001).
18. Hahn, M. W., Stajich, J. E. & Wray, G. A. The effects of selection against spurious transcription factor binding sites. *Mol. Biol. Evol.* **20**, 901–906 (2003).
19. Langley, C. H. & Ito, K. Spontaneous mutability in *Drosophila melanogaster*, in natural and laboratory environments. *Mutat. Res.* **36**, 385–386 (1976).
20. Gunsalus, K. C., Yueh, W. C., MacMenamin, P. & Piano, F. RNAiDB and PhenoBlast: web tools for genome-wide phenotypic mapping projects. *Nucleic Acids Res.* **32**, D406–D410 (2004).
21. Naclerio, G. *et al.* Molecular and genomic organization of clusters of repetitive DNA sequences in *Caenorhabditis elegans*. *J. Mol. Biol.* **226**, 159–168 (1992).
22. Keightley, P. D. & Ohnishi, O. EMS-induced polygenic mutation rates for nine quantitative characters in *Drosophila melanogaster*. *Genetics* **148**, 753–766 (1998).
23. Davies, E. K., Peters, A. D. & Keightley, P. D. High frequency of cryptic deleterious mutations in *Caenorhabditis elegans*. *Science* **285**, 1748–1751 (1999).
24. Stein, L. D. *et al.* The genome sequence of *Caenorhabditis briggsae*: a platform for comparative genomics. *PLoS Biol.* **1**, 166–192 (2003).
25. Kondrashov, A. S. & Houle, D. Genotype–environment interactions and the estimation of the genomic mutation rate in *Drosophila melanogaster*. *Proc. R. Soc. Lond. B* **258**, 221–227 (1994).
26. Higgins, D. G., Thompson, J. D. & Gibson, T. J. Using CLUSTAL for multiple sequence alignments. *Methods Enzymol.* **266**, 383–402 (1994).
27. Hill, F., Gemund, C., Benes, V., Ansorge, W. & Gibson, T. J. An estimate of large-scale sequencing accuracy. *EMBO Rep.* **1**, 29–31 (2000).
28. Richterich, P. Estimation of errors in 'raw' DNA sequences: a validation study. *Genome Res.* **8**, 251–259 (1998).
29. Denver, D. R. *et al.* Abundance, distribution, and mutation rates of homopolymeric nucleotide runs in the genome of *Caenorhabditis elegans*. *J. Mol. Evol.* **58**, 584–595 (2004).

Supplementary Information accompanies the paper on [www.nature.com/nature](http://www.nature.com/nature).

**Acknowledgements** We thank L. L. Vassilieva, S. Estes, V. Katju and C. Steding for their respective roles in propagating and maintaining the MA lines over the past 5 years; D. Ash for help with primer sequence design and DNA sequencing; and the *Caenorhabditis* Genetics Center for providing the *C. elegans* natural isolates. This work was supported by a University of Missouri Research Board grant to W.K.T., and an NIH grant to M.L. and W.K.T.

**Competing interests statement** The authors declare that they have no competing financial interests.

**Correspondence** and requests for materials should be addressed to D.R.D. ([ddenver@bio.indiana.edu](mailto:ddenver@bio.indiana.edu)).

Optimal neural population coding of an auditory spatial cue

Nicol S. Harper<sup>1,2</sup> & David McAlpine<sup>1</sup>

<sup>1</sup>Department of Physiology and UCL Ear Institute and <sup>2</sup>CoMPLEX, University College London, London WC1E 6BT, UK

A sound, depending on the position of its source, can take more time to reach one ear than the other. This interaural (between the ears) time difference (ITD) provides a major cue for determining the source location<sup>1,2</sup>. Many auditory neurons are sensitive to ITDs<sup>3,4</sup>, but the means by which such neurons represent ITD is a contentious issue. Recent studies question whether the classical general model (the Jeffress model<sup>5</sup>) applies across species<sup>6,7</sup>. Here we show that ITD coding strategies of different species can be explained by a unifying principle: that the ITDs an animal naturally encounters should be coded with maximal accuracy. Using statistical techniques and a stochastic neural model, we demonstrate that the optimal coding strategy for ITD depends critically on head size and sound frequency. For small head sizes and/or low-frequency sounds, the optimal coding strategy tends towards two distinct sub-populations tuned to ITDs outside the range created by the head. This is consistent with recent observations in small mammals<sup>6,7</sup>. For large head sizes and/or high frequencies, the optimal strategy is a homogeneous distribution of ITD tunings within the range created by the head. This is consistent with observations in the barn owl<sup>8–10</sup>. For humans, the optimal strategy to code ITDs from an acoustically measured distribution depends on frequency; above 400 Hz a homogeneous distribution is optimal, and below 400 Hz distinct sub-populations are optimal.

The ability to localize sound sources has obvious survival value, whether for prey or predator. Many vertebrates, including humans, make use of ITDs to localize sounds in the horizontal plane. These ITDs can be in the order of just a few tens of microseconds. In the Jeffress model<sup>5</sup>, these minute ITDs are encoded by an array of coincidence-detector neurons. Each neuron is tuned for (responds maximally to) an ITD within the range created by the head size (the physiological range), the precise tuning being determined by the difference in axonal conduction time from each ear. The Jeffress model, developed with human spatial hearing in mind, has received extensive support from studies in barn owls<sup>8–10</sup>, and until recently was presumed to apply to mammals<sup>11</sup>. However, the preferred ITD tuning of neurons recorded in small mammals that use ITDs for sound localization seems to lie outside the physiological range<sup>6,7</sup>. This is markedly different to the preferred ITD tuning observed in the barn owl and suggested by the Jeffress model. It is now debated whether a single unifying principle or model can any longer explain the means by which ITD is encoded across the wide range of species in which ITD sensitivity is observed.

We investigated the possibility that different coding strategies observed in different species can be explained by the demand for accurate ITD coding. For simplicity, we considered first how to encode most accurately the ITDs in the ongoing fine structure of a pure tone using a population of ITD-tuned model neurons. In mammals, fine-structure ITD sensitivity is restricted to sound frequencies below ~1,500 Hz. At higher frequencies, some ITD information can be conveyed by the envelope structure of complex sounds<sup>12</sup>; however, this seems to have relatively little impact on localization judgements<sup>2,13</sup>, and thus we only consider fine-structure ITDs.

Here, we present the optimal coding strategies for four species with different head sizes and/or different sound-frequency ranges

over which ITD sensitivity is observed: gerbil, a species with low-frequency ( $< \sim 1,500$  Hz) ITD sensitivity and a small head; barn owl, a high-frequency ( $< \sim 10$  kHz) ITD specialist with a small head; human, low-frequency ITD sensitivity with a large head; and cat, low-frequency ITD sensitivity with an intermediate head size.

We use the simplest neural model, the ITD tuning curve (that is, a function describing a neuron's mean firing rate in response to different ITDs). For pure tones, each ITD corresponds to an ongoing interaural phase difference (IPD). IPDs up to half the pure-tone period in magnitude constitute ITD as a proportion of that period. Because pure tones are periodic, IPDs beyond half a cycle of the period are subject to 'phase wrapping'. For example, an IPD of  $+0.6$  cycles is equivalent to an IPD of  $-0.4$  cycles. Although measured ITD tuning curves scale with frequency, when considered in terms of IPD they are largely invariant with frequency, being bell-shaped around a 'best IPD' (that is, the IPD that evokes maximum discharge rate; Fig. 1a). Thus, for convenience, all ITD tuning curves are represented in terms of the equivalent IPD. We approximate the IPD tuning curves with a cosine-based function (see Methods).

We assume that IPD is encoded in the neural population's spike counts within a time window, with intrinsic Poisson noise producing variability in the spike counts. The overall measure of the population's coding error is the sum of the error for each IPD, weighted by the probability of occurrence of that IPD. The measure of coding error for each IPD is the variance of the population's representation of that IPD, as calculated from Fisher information (see Methods). For each species, for each pure-tone frequency, we determine the optimal coding strategy (optimal distribution of best IPDs) by shifting systematically the best IPD of each neuron (in a population of 200) until the overall coding error is minimized.

For the probability distribution of the IPDs of a pure tone we observe that the maximum ITD an animal experiences under natural listening conditions is limited by the size of its head. The maximum IPD corresponds to the maximum ITD as a proportion of the pure-tone period, up to a limit of half a cycle. We assume that only IPDs with magnitude smaller than the maximum IPD (that is, within the physiological range) are encountered, and that all IPDs within this range are equally likely. The effect of phase wrapping on the IPD probability distribution is ignored, as including it in the model has little qualitative effect on the results. The physiological range for each tone frequency is illustrated in Fig. 1b for the cat.

The first species considered, the gerbil, has a relatively small head with a maximum ITD of approximately  $\pm 120 \mu\text{s}$ . Consequently, for every frequency at which IPD sensitivity is observed, the gerbil's physiological range of IPDs is narrow relative to the IPD tuning curve. The optimal coding strategy for a 500-Hz pure tone (Fig. 2a) takes the form of two distinct neural sub-populations, with best IPDs positioned either side of zero and beyond the gerbil's physiological range. These two sub-populations are apparent over the full range of ITD-sensitive tone frequencies (Fig. 2c), with only a slight divergence at the highest frequencies. This is consistent with recent

electrophysiological recordings made in the brainstem of the gerbil<sup>7</sup> and the midbrain of the guinea-pig<sup>6,14,15</sup>, another small mammal with low-frequency IPD sensitivity. It is clear that this solution is optimal from the Fisher information, a local measure of coding accuracy, which is highest over the slopes of the IPD tuning curves rather than at their peaks. To position the peak Fisher information within the physiological range it is therefore necessary to position peaks of IPD functions beyond the physiological range.

The solution for the gerbil could be taken to suggest that the optimal coding strategy is largely independent of frequency and involves distinct neural sub-populations. However, the solution for the barn owl indicates that this is not the case. Barn owls, with a similar maximum ITD ( $\pm 180 \mu\text{s}$ ) to the gerbil, make use of fine-structure ITD cues over a much higher frequency range ( $3\text{--}10$  kHz<sup>8-10</sup>) than mammals. Over this range, the physiological range of IPDs (Fig. 2b) is wide relative to the IPD tuning curves, and the optimal coding strategy involves, instead, a homogeneous distribution of neurons tuned to IPDs within the physiological range.

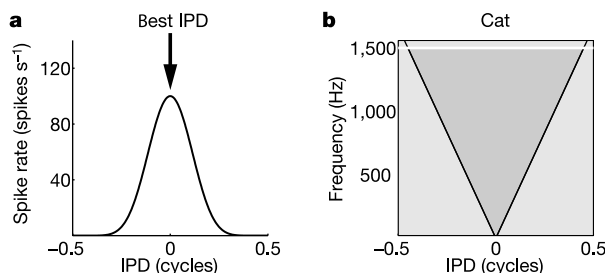


**Figure 1** Key features of model. **a**, Illustration of the IPD tuning curve used in the model. **b**, Physiological range (dark grey) of IPD in a cat, showing the limit of IPD sensitivity (white line) and the maximum IPD for each frequency (black line).

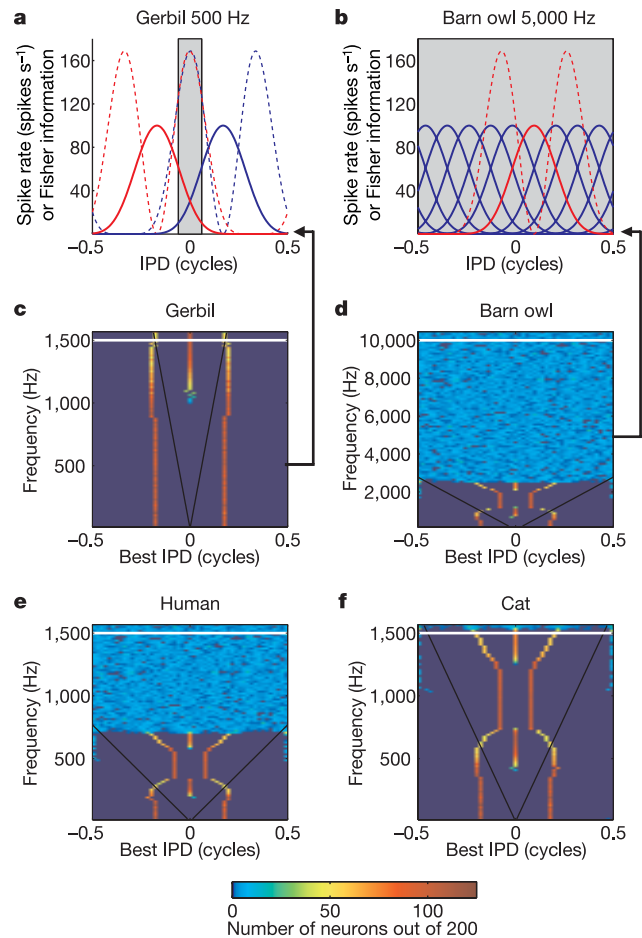


**Figure 2** Optimal distributions of tuning curves for coding IPDs. **a**, Optimal distribution of tuning curves to code the IPD of 500-Hz tones in gerbil for left (red) and right (blue) sub-populations. Dashed lines show Fisher information curves (scaled by dividing by duration of the spike-count window,  $T$ ). The grey region indicates the physiological range of IPDs, whereas vertical black lines indicate the maximum IPD. **b**, Optimal distribution for coding IPDs of 5,000-Hz tones in barn owl (sample only shown). Red lines show tuning curve (solid) and scaled Fisher information (dashed) for one neuron. **c-f**, Optimal distributions for coding pure tone IPDs in gerbil (**c**), barn owl (**d**), human (**e**) and cat (**f**). The abscissa and ordinate indicate best IPD and pure-tone frequency, respectively. For each frequency, the colour indicates the number of neurons (of 200) with that best IPD. White lines indicate frequency limit for IPD sensitivity, and black lines maximum IPD. Black arrows show how **a** and **b** illustrate the distribution at particular frequency bands in **c** and **d**, respectively.

This is consistent with physiological recordings made at all levels of the barn owl binaural pathway<sup>8–10</sup>. When the effects of phase wrapping on the IPD distribution are included in the analysis, the homogeneous distribution is maintained, save for slight fluctuations in neuron densities. The homogeneous distribution seems to be consistent with the basic tenets of the classical Jeffress model<sup>5</sup>. The solution is optimal because the slopes of IPD tuning curves, where Fisher information is maximal, always reside within the physiological range, and homogeneity is preferred because of the reciprocal term in equation (2) (see Methods). Previous general theoretical studies using relatively narrow tuning curves also

demonstrate that the optimal distribution of preferred tuning follows the probability distribution of the stimulus<sup>16</sup>.

The homogeneous solution departs from the Jeffress model in the form of the presumed coding strategy. The Jeffress model posits local coding for ITD, whereas we assume a population code, in which the slopes of functions are critical. This is consistent with a recent study of the barn owl midbrain<sup>17</sup>, which reports neural resolution of a parameter related to ITD (azimuthal location of broadband noise) to be highest over the slopes, rather than the peaks, of functions. Furthermore, although the homogeneous distribution is the optimal strategy above 3 kHz in the barn owl, below 3 kHz the solution is more complex, and distinct sub-populations are observed (Fig. 2d). Below approximately 800 Hz, the solution is essentially the same as for the gerbil. There is a paucity of data for barn owl neurons with sound frequency tuning below 3 kHz. However a recent study<sup>18</sup> reports a population of ITD-sensitive neurons with tuning for sound frequency extending down to the sub-kHz range. Although this study indicates a sub-population of neurons tuned around zero ITD, a distinct sub-population also exists with response maxima to ITDs significantly beyond the barn owl's physiological range. Distinct sub-populations and tuning beyond the physiological range are inconsistent with the Jeffress model; however, they are consistent with the optimal coding model.

The optimal coding strategies described thus far consist largely of either two distinct, opposed sub-populations tuned to ITDs beyond the physiological range, or a single homogeneous distribution lying entirely within the physiological range. For humans, however, with their relatively large head size and maximum ITD in excess of  $\pm 600 \mu\text{s}$ , the solution is more variable (Fig. 2e). For the lowest frequencies ( $< 250$  Hz) the optimal coding strategy is the same as for the gerbil, a distribution consisting of two distinct sub-populations. For the highest frequencies ( $> 700$  Hz) the homogeneous distribution is optimal. For intermediate frequencies (250–700 Hz), however, a transition occurs between the two coding strategies, with the optimal strategy consisting of several distinct sub-populations. Similarly, the solution for the cat (Fig. 2f), with a physiological range of ITDs intermediate to that of gerbil and humans, emphasizes the transition distributions.

The model indicates that a critical factor in determining the strategy for optimal coding is the relative width of the physiological range of IPDs compared with the width of individual IPD tuning curves. The model assumes the shape of the IPD tuning curve to be similar across species. Therefore, the exact form of the optimal coding strategy depends only on the maximum IPD at that frequency. As maximum IPD scales with frequency and/or head size, the panels of Fig. 2c–f are simply scaled and shifted versions of each other. However, it is likely that the optimal strategy will also depend on the exact shape of the IPD probability distribution, and to this end we measured the probability distribution of IPDs for human listeners and applied this distribution to the model. Small microphones, positioned at the entrance to each ear canal, were used to make stereo sound recordings from three human subjects interacting in a range of acoustic environments. IPD probability distributions were calculated for each frequency component in recordings from each subject–environment combination (Figs 3a–d, see Methods). The pure-tone model can be used to find the optimal coding strategy for these IPD distributions if it is assumed that ITD coding in each frequency band is optimized independently, a reasonable assumption as auditory processing is carried out within finite frequency channels up to a very high level in the auditory pathway. Figure 3e–h illustrates the corresponding solutions for each subject–environment combination. Above 400 Hz, the optimal coding strategy is a homogeneous distribution, consistent with the previous assumption of equal probability IPDs. Despite the IPD distributions being subject to the effects of phase wrapping, only small fluctuations in the homogeneous distribution were observed.

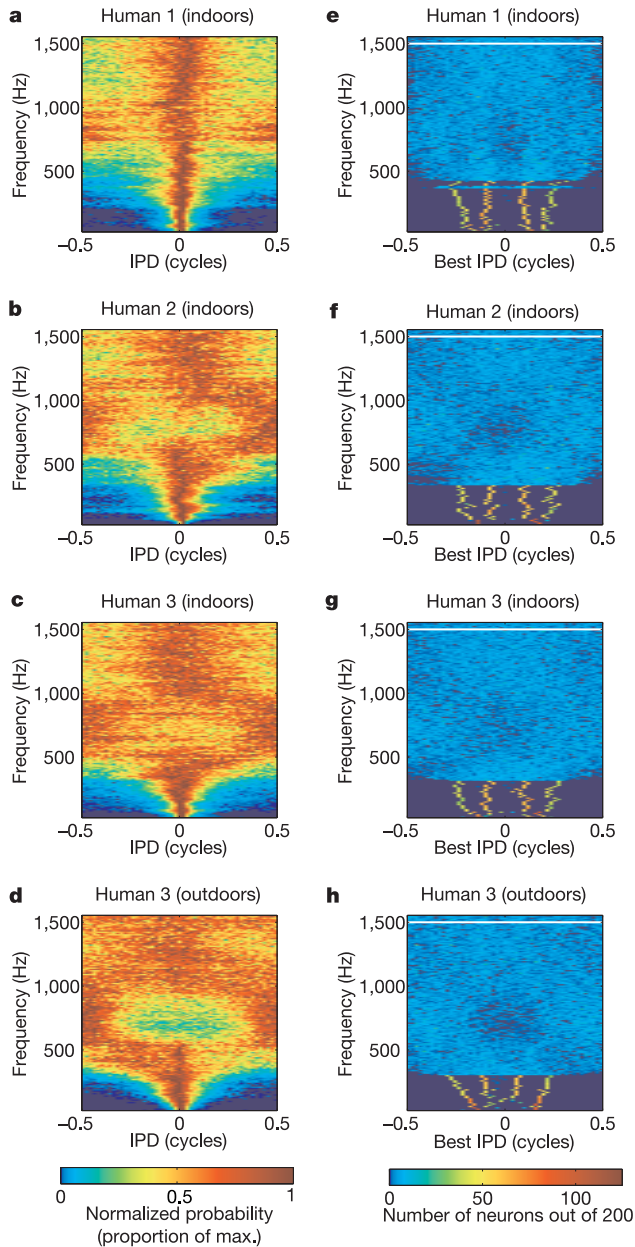


**Figure 3** Probability distributions of IPDs at different frequencies for three human subjects. **a–d**, Subjects in a room (**a–c**), and outdoors (**d**; same subject as in **c**). The IPD distribution at each frequency is normalized to maximum. The abscissa and ordinate indicate IPD and frequency, respectively. Colour indicates the normalized probability. **e–h**, Optimal distributions of best IPDs for **a–d**. The abscissa and ordinate indicate best IPD and frequency, respectively. For each frequency, the colour indicates the number of neurons (out of 200) with that best IPD. White lines indicate the frequency limit of IPD sensitivity.

Below 400 Hz, however, a modification of the two sub-population solution is optimal, with two central sub-populations and two additional, less populous, flanking sub-populations.

Although we assume ITD coding to be optimized independently for each frequency band, similar solutions are found without this assumption. If we optimize a population of model neurons to encode most accurately the ITD of a broadband noise, with the ITD tuning of each neuron modelled by a Gabor function with randomly assigned frequency, the solution is consistent with the pure-tone model (data not shown). The two sub-population solution was obtained for low-frequency-tuned neurons and small head sizes. For larger head sizes and higher frequency tuned neurons, the solution tended towards the homogeneous distribution. Furthermore, if the measure of coding accuracy is based on mutual information<sup>16</sup> rather than expected variance, it has little qualitative effect on the solutions of the models. Finally, as long as spike-rate variance is approximately proportional to mean spike rate, the same coding strategies result.

A question arises as to the developmental mechanism by which each optimal distribution could be achieved. Where the model suggests only one coding strategy across the entire frequency range at which ITDs are used (for example, 3–10 kHz in the barn owl) the optimal distribution could be hardwired, possibly by means of neural delay lines<sup>19</sup>. Another, more dynamic, mechanism is suggested by recent evidence from the gerbil of a fast glycine-mediated input that modulates the best ITD of medial superior olive neurons<sup>7</sup>. Evidence suggests that this inhibitory input can be modulated over development by the sound environment<sup>20</sup>. Such a regulatory mechanism for ITD tuning would be useful where developmental changes in head size influence which coding strategy is optimal, or where, as we predict for humans, different coding strategies are optimal for different sound frequencies.

The relatively simple model we describe provides an explanation for reported differences in neural coding of ITDs between different mammals, and between mammals and barn owls<sup>6–10,18</sup>. Assuming only the requirement of accurate coding of this auditory spatial cue, the model suggests a general framework in which to predict the coding strategy adopted by any species, depending on head size and ITD-sensitive sound frequency range. Two general categories of coding strategy were apparent: one with distinct sub-populations of ITD-sensitive neurons, and one with a homogeneous population. The model also predicts that some species, humans for example, may use different ITD-coding strategies over different sound frequency ranges. The assumption of accurate coding provides a unifying principle by which future investigations into the anatomical and physiological mechanisms responsible for ITD sensitivity may be guided. □

## Methods

### The error measure

The error measure  $V(\varphi)$  is minimized by varying the best IPDs,  $\varphi$ , of a population of model IPD-sensitive neurons, to provide for the most accurate distribution of best IPDs,  $\varphi_{\text{optimal}}$ .  $V(\varphi)$  is the expected value of the variance  $\sigma^2(\theta|\varphi)$  of the representation of IPD  $\theta$  by the spike counts of the model neurons, over a sufficiently long time window, given IPD probability distribution  $p(\theta)$ . The variance is small enough (just-noticeable difference in IPD typically  $\sim 3^\circ$ )<sup>21</sup> to ignore the angular nature of IPD  $\theta$  (angles  $\theta$  and  $\varphi$  here are in radians). Thus:

$$V(\varphi) = \int_{-\pi}^{\pi} \sigma^2(\theta|\varphi)p(\theta)d\theta \quad (1)$$

For each IPD, a lower bound on the variance  $\sigma^2(\theta|\varphi)$  in the coded IPD is given by the Cramér–Rao bound  $\sigma^2(\theta|\varphi) \geq 1/F(\theta|\varphi)$ , where  $F(\theta|\varphi)$  is the Fisher information of the population<sup>22</sup>. In the limit of a large number of  $N$  neurons the Cramér–Rao bound becomes an equality, and any bias tends to zero. Hence:

$$V(\varphi) = \int_{-\pi}^{\pi} F(\theta|\varphi)^{-1}p(\theta)d\theta \quad (2)$$

Assuming that the noise between neurons is not correlated, the Fisher information  $F(\theta|\varphi)$  of the population is the sum of the Fisher information  $f(\theta|\varphi_i)$  of each individual neuron  $i$ , where  $\varphi_i$  is a neuron's best IPD.  $f(\theta|\varphi_i)$ , for intrinsic Poisson noise, in turn depends on the IPD tuning curve,  $g(\theta|\varphi_i)$ , and the duration  $T$  of the spike-count time window. Thus the

population Fisher information is given by:

$$F(\theta|\varphi) = \sum_{i=1}^N f(\theta|\varphi_i), \text{ with } f(\theta|\varphi_i) = T \frac{[\frac{\partial}{\partial \varphi} g(\theta|\varphi_i)]^2}{g(\theta|\varphi_i)} \quad (3)$$

$V(\varphi)$  is minimized using a conjugate-gradient-based algorithm (Minimize; <http://www.kyb.tuebingen.mpg.de/bs/people/carl/code/>). It finds the minimum within 1,000 line searches, and usually fewer than 50.  $\varphi$  is initially normally distributed around 0 IPD, however the same solutions result when other initial distributions are used.

### IPD tuning curves

For the IPD tuning curve we chose the function  $g(\theta|\varphi_i)$  to provide a reasonable fit to the inner slope of a number of tuning curves recorded from the guinea-pig inferior colliculus. The exact function is:

$$g(\theta|\varphi_i) = r_{\text{max}} \left[ \frac{1}{2} + \frac{1}{2} \cos(\theta - \varphi_i) \right]^4 \quad (4)$$

The maximum firing rate  $r_{\text{max}}$ , like the window length  $T$ , is a constant that can be ignored in the optimization so long as  $r_{\text{max}}T$  is sufficiently large<sup>23</sup>. The maximum firing rates tend to be high in the auditory brainstem (>100 spikes per second), and psychophysically derived binaural integration times are long ( $\sim 100$  ms)<sup>24</sup>.

### Measuring the probability distribution of IPDs

Small microphones (Knowles FG3452) were fixed at the entrance to each ear canal in three human subjects and ambient sounds recorded over approximately 2 min. The subject–environment combinations were male 1 (Fig. 3a) or female 1 (Fig. 3b) in conversation with the experimenter walking around a room (4 × 4 × 3 m), male 2 walking in the same environment, but in the absence of conversation (Fig. 3c), and male 2 seated in the front quadrangle (100 × 50 m) of University College London, with multiple other persons in the quadrangle (Fig. 3d). For each subject–environment combination the recorded stereo sound was partitioned into sections using a 100-ms (seven standard deviations) gaussian window, shifted in 50-ms increments. A Fast Fourier transform was applied to each section for each ear, to give the phase for each frequency band. From this, the IPD for each frequency band in each section was calculated as the difference in phase between the ears. The probability distribution of IPDs across all of the sections was then obtained for each frequency band.

Received 25 February; accepted 18 June 2004; doi:10.1038/nature02768.

1. Rayleigh, L. On our perception of sound direction. *Phil. Mag.* **13**, 214–232 (1907).
2. Wightman, F. L. & Kistler, D. J. The dominant role of low-frequency interaural time differences in sound localisation. *J. Acoust. Soc. Am.* **91**, 1648–1661 (1992).
3. Kuwada, S. & Yin, T. C. T. Binaural interaction in low-frequency neurons in inferior colliculus of the cat. I. Effects of long interaural delays, intensity, and repetition rate on interaural delay function. *J. Neurophysiol.* **50**, 981–999 (1983).
4. Yin, T. C. T. & Chan, J. C. K. Interaural time sensitivity in medial superior olive of cat. *J. Neurophysiol.* **64**, 465–488 (1990).
5. Jeffress, L. A. A place theory of sound localisation. *J. Comp. Physiol. Psychol.* **41**, 35–39 (1948).
6. McAlpine, D., Jiang, D. & Palmer, A. R. A neural code for low-frequency sound localization in mammals. *Nature Neurosci.* **4**, 396–401 (2001).
7. Brand, A., Behrend, O., Marquardt, T., McAlpine, D. & Grothe, B. Precise inhibition is essential for microsecond interaural time difference coding. *Nature* **417**, 543–547 (2002).
8. Takahashi, T. & Konishi, M. Selectivity for interaural time difference in the owl's midbrain. *J. Neurosci.* **6**, 3413–3422 (1986).
9. Wagner, H., Takahashi, T. & Konishi, M. Representation of interaural time difference in the central nucleus of the barn owl's inferior colliculus. *J. Neurosci.* **7**, 3105–3116 (1987).
10. Coles, R. B. & Guppy, A. Directional hearing in the barn owl (*Tyto alba*). *J. Comp. Physiol. A* **163**, 117–133 (1988).
11. Joris, P. X., Smith, P. H. & Yin, T. C. T. Coincidence detection in the auditory system: 50 years after Jeffress. *Neuron* **21**, 1235–1238 (1998).
12. Henning, G. B. Detectability of interaural delay in high-frequency complex waveforms. *J. Acoust. Soc. Am.* **55**, 84–90 (1974).
13. Bernstein, L. R. & Trahiotis, C. Lateralization of sinusoidally amplitude-modulated tones: Effects of spectral locus and temporal variation. *J. Acoust. Soc. Am.* **78**, 514–523 (1985).
14. Skottun, B. C., Shackleton, T. M., Arnott, R. H. & Palmer, A. R. The ability of inferior colliculus neurons to signal differences in interaural delay. *Proc. Natl Acad. Sci. USA* **98**, 14050–14054 (2001).
15. Shackleton, T. M., Skottun, B. C., Arnott, R. H. & Palmer, A. R. Interaural time difference discrimination thresholds for single neurons in the inferior colliculus of Guinea pigs. *J. Neurosci.* **23**, 716–724 (2003).
16. Brunel, N. & Nadal, J. P. Mutual information, Fisher information, and population coding. *Neural Comput.* **10**, 1731–1757 (1998).
17. Bala, A. D., Spitzer, M. W. & Takahashi, T. T. Prediction of auditory spatial acuity from neural images on the owl's auditory space map. *Nature* **424**, 771–774 (2003).
18. Wagner, H., Mazer, J. A. & von Campenhausen, M. Response properties of neurons in the core of the central nucleus of the inferior colliculus of the barn owl. *Eur. J. Neurosci.* **15**, 1343–1352 (2002).
19. Carr, C. E. & Konishi, M. Axonal delay lines for time measurement in the owl's brainstem. *Proc. Natl Acad. Sci. USA* **85**, 8311–8315 (1988).
20. Kapfer, C., Seidl, A. H., Schweizer, H. & Grothe, B. Experience-dependent refinement of inhibitory inputs to auditory coincidence-detector neurons. *Nature Neurosci.* **5**, 247–253 (2002).
21. Domnitz, R. H. & Colburn, H. S. Lateral position and interaural discrimination. *J. Acoust. Soc. Am.* **61**, 1586–1598 (1977).
22. Dayan, P. & Abbot, L. F. *Theoretical Neuroscience: Computational and Mathematical Modeling of Neural Systems* (MIT Press, Cambridge, Massachusetts, 2001).
23. Bethge, M., Rotermund, D. & Pawelzik, K. Optimal short-term population coding: When Fisher information fails. *Neural Comput.* **14**, 2317–2351 (2002).

24. Culling, J. F. & Summerfield, Q. Measurements of the binaural temporal window using a detection task. *J. Acoust. Soc. Am.* **103**, 3540–3553 (1998).

**Acknowledgements** We thank C. Rasmussen for the algorithm ‘Minimize’. This work was supported by a MRC Career Establishment Grant to D.M and a MRC Bioinformatics Studentship to N.S.H.

**Competing interests statement** The authors declare that they have no competing financial interests.

**Correspondence** and requests for materials should be addressed to D.M (d.mcalpine@ucl.ac.uk).

## Sirtuin activators mimic caloric restriction and delay ageing in metazoans

Jason G. Wood<sup>1\*</sup>, Blanka Rogina<sup>2\*</sup>, Siva Lavu<sup>1</sup>, Konrad Howitz<sup>3</sup>, Stephen L. Helfand<sup>2</sup>, Marc Tatar<sup>4</sup> & David Sinclair<sup>1</sup>

<sup>1</sup>Department of Pathology, Harvard Medical School, 77 Ave. Louis Pasteur, Boston, Massachusetts 02115, USA

<sup>2</sup>Department of Genetics and Developmental Biology, University of Connecticut Health Center, 263 Farmington Ave., Farmington, Connecticut 06030, USA

<sup>3</sup>BIOMOL Research Laboratories, Inc., 5120 Butler Pike, Plymouth Meeting, Pennsylvania 19462, USA

<sup>4</sup>Department of Ecology and Evolutionary Biology, Box G-W, Brown University, Providence, Rhode Island 02912, USA

\*These authors contributed equally to this work

Caloric restriction extends lifespan in numerous species. In the budding yeast *Saccharomyces cerevisiae* this effect requires Sir2 (ref. 1), a member of the sirtuin family of NAD<sup>+</sup>-dependent deacetylases<sup>2,3</sup>. Sirtuin activating compounds (STACs) can promote the survival of human cells and extend the replicative lifespan of yeast<sup>4</sup>. Here we show that resveratrol and other STACs activate sirtuins from *Caenorhabditis elegans* and *Drosophila melanogaster*, and extend the lifespan of these animals without reducing fecundity. Lifespan extension is dependent on functional Sir2, and is not observed when nutrients are restricted. Together these data indicate that STACs slow metazoan ageing by mechanisms that may be related to caloric restriction.

Sir2-like proteins (sirtuins) are a family of NAD<sup>+</sup>-dependent deacetylases conserved from *Escherichia coli* to humans<sup>5–9</sup> (Fig. 1a) that play important roles in gene silencing, DNA repair, rDNA recombination and ageing in model organisms<sup>2,10–12</sup>. When diet is restricted (caloric restriction), lifespan is extended in diverse species, suggesting that there is a conserved mechanism for nutrient regulation of ageing<sup>13–17</sup>. In budding yeast, extra copies of SIR2 extend lifespan by 30%, apparently by mimicking caloric restriction<sup>1,18</sup>. We recently described a group of compounds (STACs) that stimulate the catalytic activity of yeast and human sirtuins, and extend the replicative lifespan of yeast cells by up to 60% (ref. 4).

To establish whether STACs could activate sirtuins from multicellular animals, we developed a cell-based deacetylation assay for *D. melanogaster* S2 cells. Unlike other classes of deacetylases, the sirtuins are insensitive to the inhibitor trichostatin A (TSA). Several classes of polyphenolic STACs, including chalcones, flavones and stilbenes, increased the rate of TSA-insensitive deacetylation (Fig. 1b). To determine whether this activity was due to direct stimulation of a Sir2 homologue, we purified recombinant SIR-2.1 of *C. elegans* and Sir2 of *D. melanogaster* and determined the effect of various STACs on enzymatic activity *in vitro* (Fig. 1c, d). In a

dose-dependent manner, resveratrol stimulated deacetylation up to 2.5-fold for SIR-2.1 (Fig. 1e) and 2.4-fold for Sir2 (Fig. 1f). As previously observed with the yeast and human Sir2 enzymes, resveratrol lowered the  $K_m$  of SIR-2.1 for the co-substrate NAD<sup>+</sup> (Fig. 1g).

Because resveratrol can significantly extend replicative lifespan in yeast<sup>4</sup>, we asked whether STACs could also extend lifespan in the metazoans *C. elegans* and *D. melanogaster*. Wild-type worms were transferred to plates containing 0 or 100 μM of resveratrol shortly after reaching adulthood. Lifespan was extended up to 14%, using

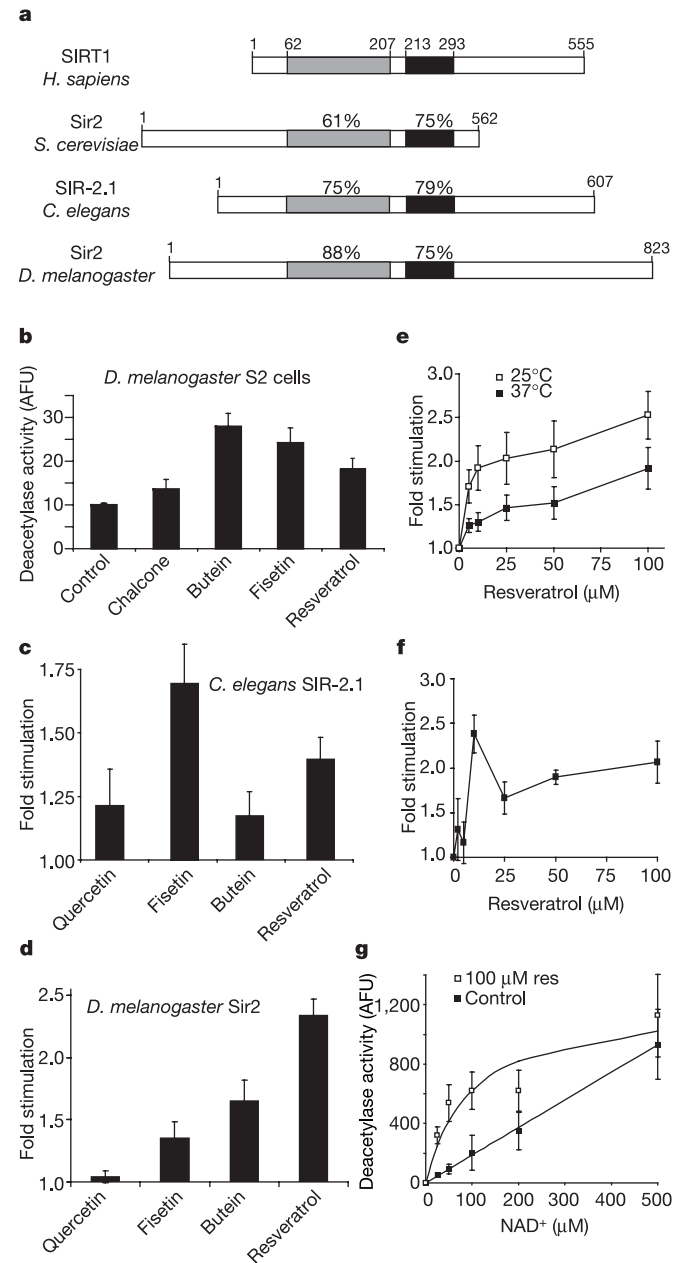


**Figure 1** Effect of polyphenolic STACs on sirtuins. **a**, Sir2 polypeptides from various species. The NAD<sup>+</sup>-binding pocket (grey), substrate-binding groove (black) and per cent homology to SIRT1 are shown. **b**, Effect of polyphenolic STACs (500 μM) on TSA-insensitive deacetylase activity in *Drosophila* S2 cells. **c**, Fold stimulation of SIR-2.1 by STACs (10 μM). **d**, Fold stimulation of *Drosophila* Sir2 by STACs (10 μM). Values are the mean of at least three determinations (±s.e.). **e, f**, Activation of *C. elegans* SIR-2.1 (**e**) and *Drosophila* Sir2 (**f**) by resveratrol (±s.e.). **g**, SIR-2.1 initial rate as a function of NAD<sup>+</sup> concentration (±s.e.). AFU, arbitrary fluorescence units.